Temporal Behavior of the Plasma Current Distribution in the ASDEX Tokamak during Lower-Hybrid Current Drive

K. McCormick, F. X. Söldner, D. Eckhartt, F. Leuterer, H. Murmann, H. Derfler, A. Eberhagen, O. Gehre, J. Gernhardt, G. v. Gierke, O. Gruber, M. Keilhacker,[a] O. Klüber, K. Lackner, D. Meisel, V. Mertens, H. Röhr, K.-H. Schmitter, K.-H. Steuer, and F. Wagner

Max-Planck-Institut für Plasmaphysik–EURATOM Association, D-8046 Garching, Federal Republic of Germany

(Received 14 April 1986)

Measurements of the time evolution of the current-density distribution in ASDEX show that lower-hybrid current drive leads to broader profiles, whereby q increases from $q \leq 1$ to $q > 1$ in the plasma central region. Simultaneously, the electron temperature is observed to peak, thus demonstrating that the lower-hybrid–driven current distribution is decoupled from the classical conductivity profile.

PACS Numbers: 52.35.Hr, 52.35.Py, 52.50.Gj, 52.55.Fa

The current-density distribution $j(r)$ within a tokamak plasma is a quantity of basic primary interest, inasmuch as it determines the local power deposition during Ohmic heating (OH) and reflects the influence of various energy-transport mechanisms. A precise knowledge of $j(r)$ is necessary, for example, to clarify its functional relationship to the electron temperature, or to elucidate the ubiquitous sawtooth instability.[1] On another matter, it has been demonstrated that MHD modes can be influenced by use of noninductive, lower-hybrid current drive (LHCD).[2-5] Thus far, the degree to which an alteration in the current profile shape is instrumental in effecting such changes has been only indirectly inferred from magnetic signals, the monitoring of MHD activity, and x-ray emission profiles. Against the background of the potential importance of LHCD mode stabilization for fusion-oriented tokamak devices, as well as from a general tokamak physics standpoint, this Letter addresses these important questions in reporting on the first detailed experimental investigations of $j(r)$ on ASDEX during OH and LHCD. The diagnostic technique employed, which utilizes a neutral-lithium-beam probe, continuously measures the local magnetic field pitch angle $\theta_p = \tan^{-1}(B_p/B_T)$ at the intersection between the beam and the optical axis of the detecting system (Fig. 1) (details in McCormick *et al.*[6,7]). By use of $\theta_p(r)$—gained by radial scanning of the beam from shot to shot—and the known toroidal field $B_T(r)$, the poloidal field $B_p(r)$ is derived, from which $j(r)$ is calculated using Ampère's law.

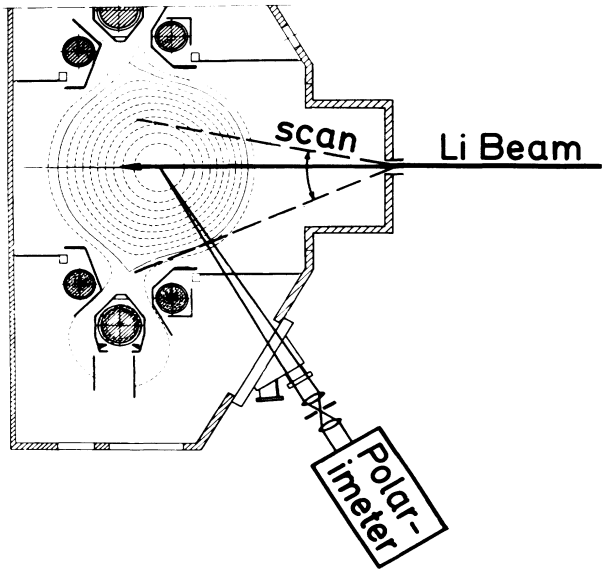

FIG. 1. Diagnostic layout on ASDEX.

Two LHCD scenarios are considered—cases (a) and (b), conditions for the latter being shown in brackets—whose parameters are summarized in Table I (plasma radius $a \sim 39.4$ cm). P_{rf} is the injected power: Propagating waves are launched with a spectrum characterized by the refractive index $\bar{N}_\parallel$ with a FWHM $\Delta N_\parallel$.[8] ASDEX is operated in H_2 [D_2] in the divertor configuration.

As seen in Fig. 2, initiation of LHCD leads to a concomitant drop in loop voltage V_L to nearly zero, showing that the plasma current is almost entirely carried by the rf. For case (a) both the diamagnetic beta $\beta_{p\perp}$ (sensitive only to the perpendicular energy) and $\Lambda + 1$ ($= \beta_p + l_i/2$, measured by poloidal flux loops) are observed to increase, in contrast to (b) where the increase in $\beta_{p\perp}$ is juxtaposed against an initial augmentation of $\Lambda + 1$ succeeded by a gradual decrease throughout the remainder of the rf pulse. Case (b) is further characterized by the immediate development of low-level MHD activity, followed within 400–600 ms after rf turnon by a much

TABLE I. Experimental parameters.

	$\bar{n}_e$ (cm^{-3})	I_p (kA)	B_T (kG)	$q(a)$	P_{rf} (kW)	$\bar{N}_\parallel$	$\Delta N_\parallel$
(a)	7×10^{12}	292	21.2	3.4	400	1.65	0.7
(b)	1.2×10^{13}	312	23.4	3.5	870	1.87	0.94

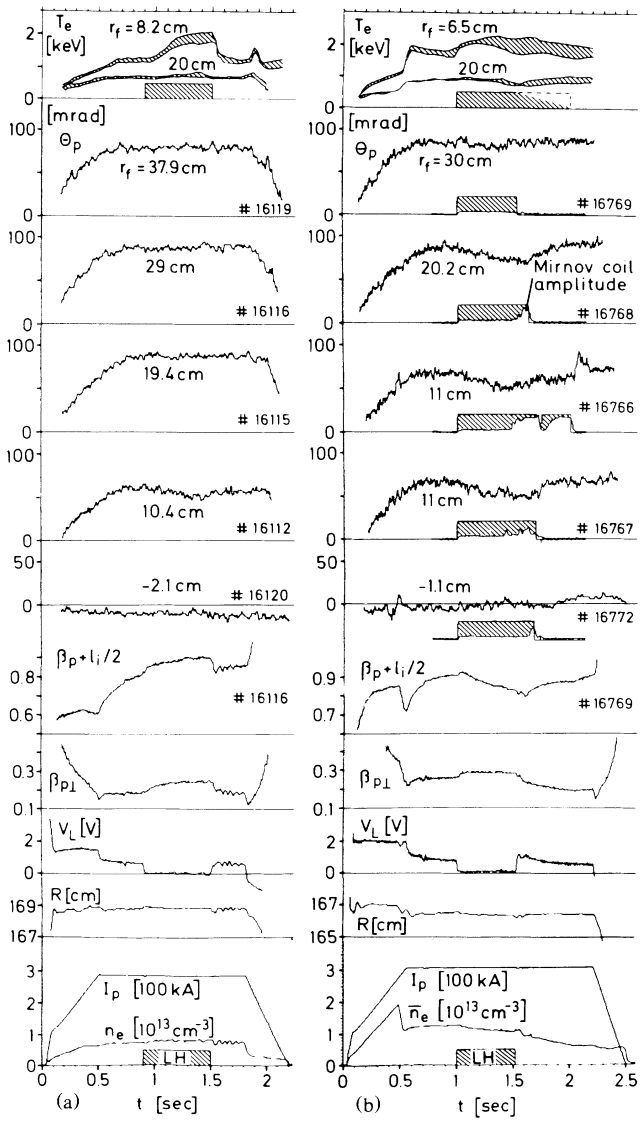

FIG. 2. Time history of T_e at two points, the experimentally measured traces of pitch angle θ_p, the magnetic signals $\beta_p + l_i/2$ and $\beta_{p\perp}$, V_L, major radius R, plasma current I_p, and line density $\bar{n}_e$. In (b) the LHCD period is shown for each discharge, as well as the amplitude of the MHD oscillations registered by a Mirnov coil.

more distinct $m/n = 2/1$ mode—which eventually triggers rf turnoff through increased power reflection. Further, the traces of pitch angle θ_p (Fig. 2) for $r_f = 11$–30 cm generally all decrease continously up to the onset of the strong $m = 2$ activity, indicating that during this time the current $I(r_f)$ contained within the flux tube of radius r_f is steadily becoming smaller, i.e., the $j(r)$ profile is broadening. In case (a) this trend is visible in $\theta_p(t)$ only for the $r_f = 10.4$-cm curve; moreover, no MHD oscillations are detected.

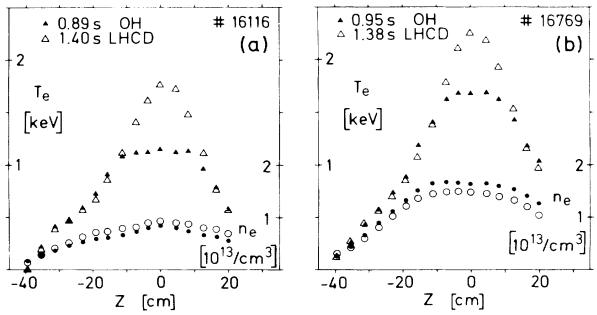

FIG. 3. T_e and n_e profiles for the OH and LHCD phases.

The electron temperature T_e is measured by a 60-Hz pulsed Thomson scattering system at sixteen points along an off-axis vertical chord. The two T_e traces (Fig. 2 —the variation over the discharge series is indicated) for the points nearest the plasma center and at midradius illustrate that LHCD has preferentially heated electrons in the plasma middle, leading to a pronounced peaking of the T_e profile as documented in Fig. 3. For the OH phase, with use of $T_e(r_f)$ in conjunction with Spitzer (Sp) or neoclassical (neo)[9] conductivity under the assumption that Z_{eff} and the electric field are independent of radius, the case-(b) Sp/neo values for Z_{eff} and $q(r=0)$ are computed to be $\sim 3.8/1.9$ and $\sim 0.92/0.54$, respectively. Z_{eff} cannot be estimated for (a) because of the presence of suprathermal electrons during OH; $q(0)$

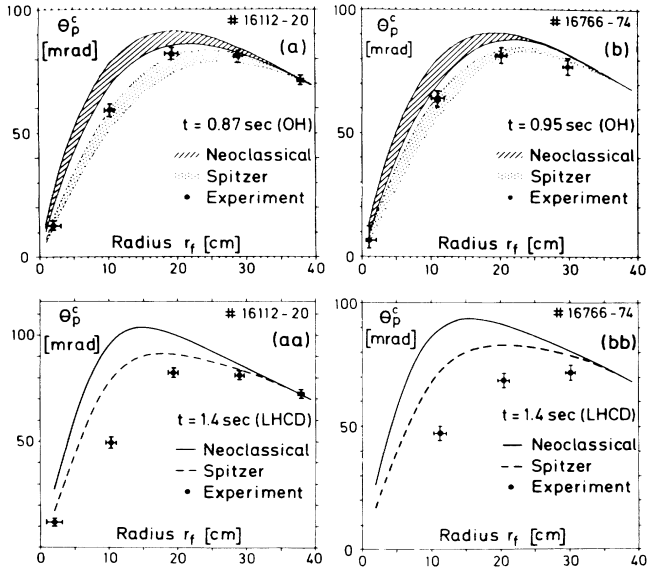

FIG. 4. Comparison among the pitch-angle profiles from $T_e(r)$, for neoclassical or Spitzer conductivity, and θ_p^c from experiment for OH (top) and LHCD (bottom). The OH curve spread reflects the shot-to-shot variation in T_e; an averaged T_e profile is used for LHCD. For display convenience, the $r_f = -2.1$ cm $[-1.1$ cm$]$ points have been mirror plotted.

is calculated to be $\sim 0.96/0.51$.

In Fig. 4 (top) a comparison between the OH Sp and neo θ_p profiles and the experimental θ_p^c points (adjusted to cylindrical geometry) shows better overall agreement with the Spitzer values. This is surprising since trapped electrons should be important ($\nu_e^* \ll 1$). However, the neoclassical curves imply that $q(0) \ll 1$. Introduction of a, say, $q \geq 1$ limitation—synonymous with the imposition of a central anomalous resistivity zone—would reduce the differences between the Sp and neo θ_p curves to within the experimental uncertainties. Graphically, this is apparent when we consider that a line drawn through the origin and the θ_p^c points at $r_f \sim 10.4$ cm [11 cm] roughly defines the upper bound of the region in which all θ_p^c values must fall if $q \gtrsim 1$ is to be fulfilled. In essence, the present data base is not well suited to a decision as to which conductivity model is more correct.

During LHCD (Fig. 4, bottom) not even the Spitzer curve describes the experimental points, unequivocally demonstrating that $j(r)$ has been decoupled from the temperature profile, i.e., classical conductivity is no longer instrumental in governing the current distribution.

The experimental values of $I(r_f) = 5 r_f B_T \tan\theta_p^c$ and $q(r_f) = r_f / R \tan\theta_p^c$ may be determined from Fig. 5, where θ_p^c is plotted for both discharge phases. The spline curves chosen to connect the θ_p^c points are motivated by the Sp and neo profiles of Fig. 4, and by other more detailed Li-beam measurements[10]—performed on OH discharges with parameters very close to those of (a) and (b)—which show in particular that $\theta_p^c(r_f \lesssim a/4)$ has a nearly constant slope, yielding $1.0 > q(r_f \lesssim a/4) > 0.9$. In the present measurements, $q(0)$ is not well characterized because of the proximity of the innermost point to the magnetic axis and the otherwise dearth of points for $r_f < a/4$; taking the extremes of the error bars for both the radial position and magnitude of θ_p^c gives (a) $q(0) = 0.94^{+0.15}_{-0.46}$ and (b) $q(0) = 0.93^{+0.2}_{-0.55}$. The changes in $I(r_f)$ and $q(r_f)$ caused by LHCD can be deduced with greater accuracy, since only the noise level of the signal (box height) need be considered. Thus, in (a) current is distinctly being redistributed from the center outwards for $r_f < a/2$, while in (b) the current profile broadening is more pronounced, being detectable even at $r_f \sim 0.75a$. Further, $\Delta q(r_f \sim a/4)$ is found to be (a) $+0.2 \pm 0.04$, and (b) $+0.4 \pm 0.04$, which should also approximately describe $\Delta q(0)$ given that $\Delta q(r_f < a/4)$ is roughly proportional to $\Delta q(r_f \sim a/4)$ as drawn in Fig. 5.

The spatial variation of q corresponding to the θ_p^c curves of Fig. 5 are presented in Fig. 6 along with the associated $j(r)$ profiles. In (b), the $q(\mathrm{OH}) = 1$ radius is ~ 10 cm, in agreement with the electron-cyclotron-emission (ECE) sawtooth (ST) inversion radius of 11.4 ± 1.7 cm. (Soft-x-ray diagnostics were not available for ST corroboration.) The diagnostic response time (~ 10 ms) is greater than the ST period (5 ms); hence, changes in q on this time scale cannot be resolved. No ST were detected by ECE in (a); they are possibly masked by emission from suprathermal electrons already present in the OH phase. In both cases, during LHCD $q(0)$ clearly increases—to greater than 1, if one uses the $q^{\mathrm{OH}}(0)$ results of Ref. 10 cited above. These measurements thus support the conjecture made elsewhere,[2,3] and the general experience on ASDEX,[5] that exclusion of the $q = 1$ zone by current profile broadening is the driving mechanism behind LHCD sawtooth suppression.

The change in time of $j(r)$, expressed in terms of the internal inductance l_i (computed from the θ_p^c profiles of Fig. 5), is depicted in Fig. 7 as $\Delta l_i/2 = (l_i^{\mathrm{LH}} - l_i^{\mathrm{OH}})/2$. In (a) $\Delta l_i/2$ reaches a plateau of $\sim -0.02 \pm 0.014$ within 200–300 ms after rf turnon. In contrast, in (b) $\Delta l_i/2$ de-

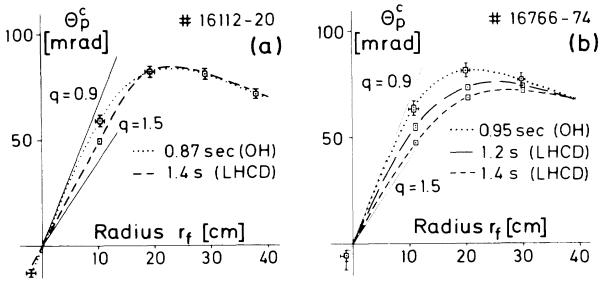

FIG. 5. Experimental θ_p^c curves. The horizontal error bars account for the uncertainty in radial position due to geometrical considerations (box width) and an estimated ± 1 cm uncertainty in the magnetic axis position (error flags). Vertically, the mean deviation of θ_p over 50 ms (box height) and the base-line error (flags) are denoted. In (b), $\theta_p^c(r_f = a)$ is calculated; the $\theta_p^c(r_f = -1.1$, LHCD) point is not used because of large error bars. The lines for θ_p^c corresponding to q values of 0.9 and 1.5 are indicated.

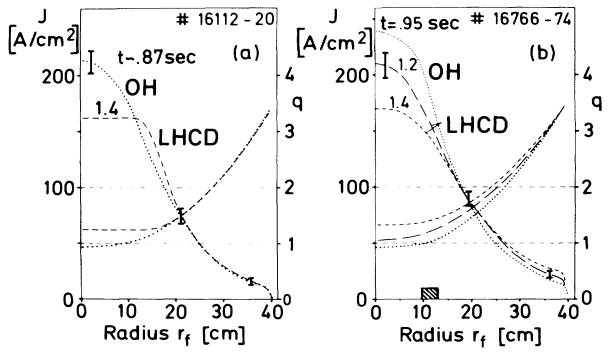

FIG. 6. Current density $j(r)$ and cylindrical q profiles derived from the θ_p^c curves of Fig. 5. The $j(r)$ error flags consider only the θ_p^c noise level, indicating the degree to which the LHCD-generated change in $j(r)$ is resolved. Note that within these limits only those $j(r)$ profiles are allowed whose integrals yield the θ_p^c points of Fig. 5. Error bars for $q(0)$ and $\Delta q(0)$ are discussed in the text. The hatched area in (b) denotes the ECE sawtooth inversion region.

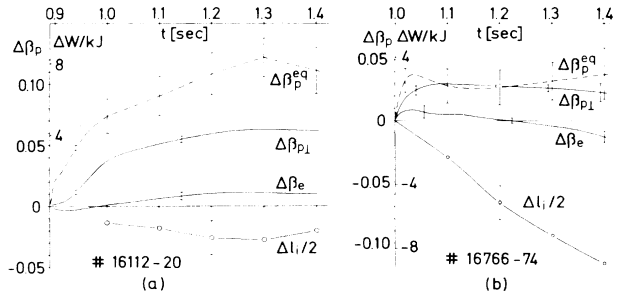

FIG. 7. LHCD-produced changes in l_i, β_e, $\beta_{p\perp}$ and β_p^{eq}. W is the increment in kilojoules. OH values: $l_i = 1.2 \pm 0.1$ [1.2], $\beta_e \sim 0.05$ [0.13], $\beta_{p\perp} \sim 0.19$ [0.26], and $\beta_p + l_i/2 = 0.81$ [0.92].

creases almost linearly over the entire time span, attaining a value of ~ -0.12 after 400 ms. Comparison of the change in equilibrium poloidal beta $\Delta\beta_p^{eq} = \Delta(\Lambda + 1) - \Delta l_i/2$ with $\Delta\beta_{p\perp}$ indicates a nearly isotropic plasma pressure in (b) and a strong anisotropy ($\Delta\beta_p^{eq} > \Delta\beta_{p\perp}$) in (a) in favor of the component parallel to the magnetic field; further, there is a greater disparity between $\Delta\beta_p^{eq}$ and $\Delta\beta_e$ (β_e is the thermal electron poloidal beta) in (a) than for (b). These $\Delta\beta$ trends are in concord with the density-dependent formation and thermalization of suprathermal electrons seen with LH heating spectra,[11] thus lending credulity to the computed Δl_i values.

Examination of the magnetic signals of Figs. 2 and 7 also serves to illustrate the value of a direct $j(r)$ measurement. In (a), the quantity "Δl_i"$/2 = \Delta(\Lambda + 1) - \Delta\beta_{p\perp}$ remains positive throughout the discharge (in the range $+0.02$–0.03) from which one might erroneously conclude—without precise knowledge of the energy anisotropy—that the current distribution has narrowed. In (b), the peaking of $\Lambda + 1$ shortly after LHCD initiation is now seen to come about from the rapid ($\sim$25-ms) formation of suprathermal electrons, accompanied by a slower relaxation of the current profile.

In conclusion, the now-documented ability of LHCD to decouple $j(r)$ from $T_e(r)$ should lend impetus to a potentially promising field of application for LH waves; for example, beta limitations arising from inductively driven $j(r)$ profiles may possibly be extended with the implementation of LH current profile shaping. That some control over the exact form of current redistribution can be achieved is demonstrated by cases (a) and (b), where $\Delta q(a/4)$ is similar ($+0.2$ vs $+0.4$), but the decrease in l_i is vastly different (-0.04 vs -0.24)—corresponding to a change in $j(r)$ either confined to $\lesssim a/2$ or extending over the entire plasma. The desirability of detailed $j(r)$ shaping is evidenced by the strong $m = 2$ tearing modes driven by the case-(b) profiles, and the experience on ASDEX that this problem, for a (b)-type rf spectrum, is exacerbated when $q(a)$ is reduced. It remains a point of further investigation to clarify the roles which density and the rf spectrum play in determining the differences between (a) and (b).

[a]Present address: JET Joint Undertaking, England.

[1]S. von Goeler *et al.*, Phys. Rev. Lett. **33**, 1201 (1974).

[2]D. van Houtte *et al.*, Nucl. Fusion Lett. **24**, 1485 (1984).

[3]F. Parlange *et al.*, in *Proceedings of the Twelfth European Conference on Controlled Fusion and Plasma Physics, Budapest, 1985* edited by L. Pocs and A. Montvai (European Physical Society, Petit-Lancy, Switzerland, 1985), Vol. 2, p. 172.

[4]J. E. Stevens *et al.*, in Ref. 3, Vol. 2, p. 192.

[5]F. Södner *et al.*, in *Proceedings of the Thirteenth European Conference on Controlled Fusion and Plasma Physics, Schliersee, 1986,* edited by G. Briffod and M. Kaufmann (European Physical Society, Petit-Lancy, Switzerland, 1986), edited by G. Briffod and M. Kaufmann (European Physical Society, Petit-Lancy, Switzerland, 1986), Vol. 2, p. 319.

[6]K. McCormick *et al.*, in *Proceedings of the Eighth European Conference on Controlled Fusion and Plasma Physics, Prague, 1977,* edited by P. Sunka (International Atomic Energy Agency, Vienna, Austria, 1978), p. 140.

[7]K. McCormick *et al.*, in Ref. 3, Vol. 1, p. 199.

[8]F. Leuterer *et al.*, Plasma Phys. **27**, 1399 (1985).

[9]S. P. Hirschman and D. J. Sigmar, Nucl. Fusion **21**, 1079 (1981).

[10]K. McCormick *et al.*, in Ref. 5, Vol. 2, p. 323.

[11]F. Söldner *et al.*, in *Course and Workshop on Applications of rf Waves to Tokamak Plasmas, Varenna, 1985,* edited by S. Bernabei, U. Gasparino, and E. Sindoni (International School of Physics "Piero Caldriola," Milan, 1985), Vol. 2, p. 740.